State-Specific Rotational Energy Transfer in OH ($A^2\Sigma^+$, $v' = 0$) by some Combustion-Relevant Collision Partners

A. Jörg[*], U. Meier, R. Kienle, and K. Kohse-Höinghaus

DLR-Institut für Physikalische Chemie der Verbrennung, Pfaffenwaldring 38–40, W-7000 Stuttgart 80, Fed. Rep. Germany

Abstract. State-to-state rotational energy transfer (RET) coefficients were determined for inelastic collisions of OH ($A^2\Sigma^+$, $v' = 0$) with N_2, CO_2, and H_2O at 300 K. The experimental procedure described previously allows the direct evaluation of state-specific RET coefficients from time-resolved laser-induced fluorescence (LIF) measurements without any assumptions on the RET. The results show strikingly different RET behaviour for the three collision partners. The data can serve as a basis for a comparison with dynamic collision models.

PACS: 34.50

Laser-induced fluorescence is one of the established techniques for the determination of minor species concentrations and of temperature in combustion [1]. In particular, two-dimensional LIF measurements in practical combustion environments offer the invaluable chance of acquiring direct, instantaneous structural information on the particular combustion situation [2–5]. One of the key problems associated with the quantitative interpretation of LIF experiments is the competition of the fluorescence emission with collision processes. This can render quantitative instantaneous two-dimensional LIF measurements in turbulent combustion situations difficult as temperature and chemical composition, which determine the local non-radiative decay rate of a laser-excited state, can vary drastically throughout the plane of observation.

Non of the various known LIF strategies is under all conditions of interest completely insensitive to collisions. A measurement of the effective fluorescence lifetime – which is a net observable result of radiative and collisional processes – can provide the necessary calibration for a quantitative interpretation of LIF signals. Although time-resolved LIF detection can be accurately performed in single-point measurements, even if this may require sub-nanosecond technology [6, 7], this approach can, at present, not easily be transferred

to two-dimensional LIF applications. Some ideas are emerging which may help to overcome this problem [8, 9]. Also, several other strategies for quantitative two-dimensional LIF measurements have been described. For the application of linear LIF in turbulent combustion, a selection of lines is proposed [10], which allows a partial compensation of population and quenching contributions to the LIF signal, thus making quenching correction unnecessary. Predissociative [11, 12] or saturated [13, 14] LIF are less sensitive to collisions than linear LIF, but their range of application for quantitative measurements is also limited. It has recently been shown that already at moderate pressures, RET in the electronic ground state may be of significant influence for the detection of OH with predissociative LIF [15]. For saturated LIF, a quantitative interpretation of measured LIF signals is, in general, not possible without exact knowledge of inelastic energy transfer coefficients, especially at high pressure [16].

Given the difficulties and limitations of all LIF techniques in view of their application to quantitative two-dimensional imaging in turbulent flames, it is often advisable to identify the experimental strategy best suited to the specific problem by computer modeling before performing the actual experiment. This has already been attempted in several cases for the detection of OH radicals [17–21]. Unfortunately, the models used for this purpose are largely based on estimates for collisional energy transfer rates as accurate experimental data are often not available.

Whereas a considerable number of investigation has contributed to the present knowledge on electronic quenching for various combustion-relevant radicals and collision partner [22–25], only a few combustion-oriented studies on RET have been performed to date. For the important OH radical, for example, predominantly total rotational energy transfer has been investigated. Total RET coefficients, which represent the overall effect of all RET processes out of (and back into) one selected quantum state, have been determined for the OH ($A^2\Sigma^+$, $v' = 0$) state at flame temperatures for N_2 and Ar [26] as well as H_2O [27] as collision partners and at 300 K for N_2 and O_2 [28]. In contrast, the only investigations on state-to-state RET in OH known to us – apart from our own work [29, 30] – are those of Lengel and Crosley

---

[*] A. Jörg is now with IBM Corporation, Frankfurt, Fed. Rep. Germany

[31] for the OH ($A^2\Sigma^+$, $v' = 0$) state, where energy transfer by N_2, H_2, and Ar was studied, and of Wysong et al. [32] for OH ($X^2\Pi_i$, $v'' = 2$) with He as collision partner.

We have recently developed a method which allows to determine state-to-state RET coefficients directly – with no need for further assumptions on the RET – from time-resolved fluorescence measurements [29, 30]. Experimental results on RET in OH ($A^2\Sigma^+$, $v' = 0$) with He and Ar at room temperature obtained with this method [29] are in excellent agreement with quantum scattering calculations [33, 34]. In the present study, we applied this method to determine state-to-state RET coefficients for OH ($A^2\Sigma^+$, $v' = 0$) at 300 K with three important flame constituents, N_2, CO_2, and H_2O. The aim of this study as part of a series of investigations [29, 30, 33, 35] is to provide a firmer basis for the development of detailed models which may be used for the selection of suitable experimental strategies for LIF measurements and eventually for their quantitative interpretation.

1 Experiment and Data Evaluation

The method and experimental set-up have previously been described in detail [29, 30]. Here, only some features of importance for the present experiments shall be given.

1.1 Experimental Procedure

For the determination of one state-to-state RET coefficient[1], two time-dependent fluorescence signals have to be measured: one originating directly from the laser-excited fine structure level, the other from a level populated by collisions. Following the data analysis presented in [29], the rate coefficient k_{if} for RET from initial state i to final state f can under our conditions be determined by an extrapolation technique. Neglecting multiple collisions to a first approximation, a single-collision RET coefficient k_{if}^s can be introduced into the differential equation that describes the time-dependent collision-induced population N_f of OH in the final state f,

$$\frac{dN_f}{dt} = N_c N_i k_{if}^s - \frac{N_f}{\tau_f} . \tag{1}$$

Here, N_c is the number density of the collider, N_i that of OH in the initial state i, and τ_f is the state-specific natural lifetime. In the actual experiment, the coefficient k_{if}^s is, however, a time-dependent quantity, as the probability for multiple collisions will increase with increasing time at a given pressure. k_{if}^s approaches the true RET coefficient k_{if} at infinitely low collision probability or, correspondingly, at time zero,

$$k_{if} = \lim_{t \to t_0} k_{if}^s . \tag{2}$$

For sufficiently low pressures and/or short observation times, the dependence of k_{if}^s on time t can be approximated by a linear function, the intercept of which yields k_{if} (see model calculations and Fig. 3 in [29]).

Our approach requires in summary that at time zero only one fine structure level is populated, and that fluorescence signals arising from both states i and f are detected with appropriate spectral and temporal resolution.

In our experiment, we chose isolated lines in the S_1 branch[2] for excitation of two different initial states: The $F_2(4)$ and $F_2(5)$ levels were populated by excitation of the $S_1(2)$ and $S_1(3)$ transitions, respectively. The corresponding fluorescence from the laser-excited level was monitored detecting the $R_2(3)$ or $R_2(4)$ line. For all collision partners, RET coefficients for transitions form the $F_2(4)$ level to $F_1(n)$ with $n = 0$–5 and to $F_2(m)$ with $m = 1, 3, 5$ as well as for transitions form the $F_2(5)$ level to $F_1(n)$ with $n = 0$–4 and $F_2(m)$ for $m = 1, 3, 4$ were determined. For this purpose, the time-dependent fluorescence intensities of 11 lines were measured at the respective spectral line centers, in particular $P_1(1')$, $Q_1(1, 1')$, $P_1(2)$, $O_2(4)$, $S_1(1)$, $P_2(4, 4')$, $O_2(5)$, $R_2(3)$, $P_1(5)$, $R_2(4)$, and $Q_1(5, 5')$. As a result, 9 coefficients could be obtained for $F_2(4)$ and 8 coefficients for $F_2(5)$ excitation from the matrix of 10 possible state-to-state coefficients with $n = 0$–5, $m = 1$–5, $f \neq i$.

In some cases, fluorescence lines blended by the corresponding satellites had to be monitored. As an example, the population of the $F_2(1)$ level was obtained from the fluorescence signals for the combined $Q_1(1, 1')$ structure and the $P_1(2)$ line: The intensity of the $Q_1(1)$ line was calculated from the measured $P_1(2)$ intensity and then subtracted from the measured intensity of the $Q_1(1, 1')$ structure. This procedure was applicable as the separation of the lines and their satellites was small and as the transmission of the monochromator was constant over the wavelength range of the entire structure. An examination of this approach was possible for the case of $P_2(4, 4')$, $S_1(1)$, and $O_2(5)$ where the $F_2(3)$ and $F_1(3)$ populations could be evaluated either directly from the $S_1(1)$ and $O_2(5)$ intensities, respectively, or by subtraction involving either one of these two lines and the intensity of the $P_2(4, 4')$ structure; the results of both the direct and the subtraction schemes were in good agreement.

The population of the $F_1(5)$ level was also obtained by subtraction measuring the $Q_1(5, 5')$ and $R_2(4)$ fluorescence intensities. This approach failed, however, when the population in $F_2(5)$ was high with respect to the one in $F_1(5)$, namely for $F_2(5)$ excitation at short times. Furthermore, our spectral resolution was not sufficient for the detection of fluorescence from the $F_2(2)$ state. For these reasons, the coefficients for RET from both initial levels to $F_2(2)$ as well as for RET from $F_2(5)$ to $F_1(5)$ could not be determined from time-resolved fluorescence measurements at a fixed spectral position. Instead, they can in principle be obtained from fluorescence *spectra* if a reduction in time resolution (and accuracy) can be accepted, as was shown for He and Ar as collision partners [29, 30].

1.2 Experimental Arrangement

The measurements were performed in a discharge flow reactor using a Nd:YAG laser-based LIF setup [29]. Typical operation conditions for the laser system, the detection channel and the flow reactor will be described successively.

---

[1] In this work, RET is used for collision processes within one vibrational level of a specific electronic state which are inelastic with respect to rotational quantum number and/or fine structure level

[2] We follow the nomenclature of Dieke and Crosswhite [36]

The frequency-doubled radiation of a Nd:YAG laser-pumped dye laser using sulforhodamine 101 dye excited the $S_1(2)$ or the $S_1(3)$ transition of the OH ($A^2 \Sigma^+ - X^2 \Pi_i$) 0–0 band. Typical pulse energies were 6–8 mJ (in a 6 ns FWHM pulse). The laser beam was unfocussed with a beam diameter of 8 mm to avoid diffusion of excited OH out of the observation volume. The spectral width of the laser of 2 cm^{-1} (FWHM) was considerably larger than the Doppler width of OH at 300 K (0.1 cm^{-1}). A polarization scrambler was used to ensure a spatially isotropic fluorescence distribution [29].

The fluorescence was monitored at right angles to the laser beam direction using two different detection systems: a broadband reference channel and the channel which detected the spectrally resolved single-line fluorescence. The system with the higher resolution used a 640 mm monochromator (Jobin Yvon HR 640). The fluorescence was collected with a $f/3.75$ lens ($f = 150$ mm) and imaged onto the slit (2 mm height × 50 μm width) with a $f/2.5$ lens ($f = 100$ mm). Three mirrors rotated the image by 90° so that the slit height determined the length of the observation volume in the direction of the laser beam. The spectral resolution in this arrangement was 3.5 cm^{-1} (FWHM of the slit function). The spectral positions of the OH lines were controlled before each set of experiments. The fluorescence signal was detected by a photomultiplier (Valvo XP2020Q) and registered either with a transient digitizer (Tektronix 7912 AD, 400 MHz) or a boxcar integrator (Stanford Research Systems SR 250). Typically the time interval from 0–200 ns was monitored. If necessary, calibrated neutral density filters (Melles Griot) were used to attenuate the signal. Depending on the particular transition, the fluorescence signals of 300–6000 laser shots were averaged to improve the signal-to-noise-ratio.

The broadband reference signal, which is proportional to the total number density of electronically excited OH radicals, served as a detector of changes in the operation conditions of the flow reactor and the optical system (e.g. fluctuations in radical production efficiency, in laser wavelength or power density). Scattered light at the laser wavelength was suppressed with bandpass filters (Schott WG 320, 6 mm). The fluorescence was collected with a $f/1$ lens ($f = 50$ mm) and monitored with a photomultiplier (RCA 1P28A) and a second boxcar integrator. A gate width of 100 ns and a delay of 150 ns were used with respect to the onset of the laser pulse for an additional discrimination against scattered laser light. Each set of averaged, spectrally resolved, time-dependent fluorescence signals was divided by the corresponding reference signal prior to the evaluation of state-specific OH number densities. If the reference signal changed by more than 15% throughout a series of measurements, these were discarded.

The flow reactor consisted of a 300 mm long quartz tube of 30 mm diameter which was placed inside a vacuum housing. Four windows at angles of 90° in the bottom part of the housing (beneath the reactor tube) allowed optical access for the laser and the detection system. OH radicals were generated in the reaction of H atoms with NO$_2$; H atoms were produced in a microwave discharge in a flow of He which contained 1–3% H$_2$. A mixture of 5% NO$_2$ in He was added downstream of the discharge, allowing for sufficient reaction time before the observation volume. The loss of radicals at the reactor walls was minimized by a surface

pretreatment with a 10% aqueous HF solution. The flow reactor operated typically at flow rates of 1–4 slm and pressures of 0.8–5 mbar. Flow rates were measured with mass flow controller (Tylan FC 280S); for H$_2$O as collision partner, a mass flow meter (Hastings EALL 500) was used. The pressure was measured with a capacitance manometer (Baratron 0–10 mbar).

For both $F_2(4)$ and $F_2(5)$ excitation and for each collision partner, the RET coefficients were determined from 100–150 independent experiments at different pressures and gas compositions. The combined partial pressures of H$_2$ and NO$_2$ were less than 1% in all experiments. In the evaluation of the measurements with N$_2$, CO$_2$, and H$_2$O as collision partners, the contribution of He to the RET had to be considered as He was used as carrier gas in these experiments. RET coefficients for OH ($A^2 \Sigma^+$, $v' = 0$) with He had been measured separately [29] so that the He contribution could be subtracted. In the experiments with N$_2$, a pressure range of 1–3.7 mbar was covered, the contributions of RET by He to the measured coefficients were below 20% in most cases. For CO$_2$, pressures of 0.8–3.3 mbar were used. The contribution of He RET was on average higher than for N$_2$, typically 10–40%. This was caused by the more unfavourable ratio between electronic quenching and RET: due to the efficient quenching, the CO$_2$ partial pressure had to be kept low to provide sufficient fluorescence intensity. RET by H$_2$O was investigated at pressures of 0.8–2.5 mbar. H$_2$O was introduced from a heated (40° C) reservoir, its mole fraction was limited by the achievable partial pressure. Depending on total pressure, the contribution of the RET by the He carrier gas changed thus from 5–50%. Most of the measurements were therefore performed at pressure below 1.2 mbar.

2 Results

RET coefficients for OH ($A^2 \Sigma^+$, $v' = 0$) upon excitation of $F_2(4)$ and $F_2(5)$ were determined for N$_2$, CO$_2$ and H$_2$O. These are the main constituents of the burnt gases in most hydrocarbon flames. The RET coefficients for the two excited transitions and the three collision partners are summarized in Fig. 1. This figure is organized as follows. The length of the bars corresponds to the magnitude of the RET coefficient; the x-axis shows the rotational quantum number N of the final state. The bars symbolizing the RET coefficients are grouped symmetrically around the quantum states: To the left, transitions with unchanged symmetry[3] ($F_2 \leftrightarrow F_2$) are shown, to the right those with $F_2 \leftrightarrow F_1$. The upper part shows RET following $F_2(5)$ excitation, the lower corresponds to $F_2(4)$ excitation.

Several aspects are striking in the comparison of RET by the different collision partners. The total transfer out of the initial state is for H$_2$O about a factor of 4 and for N$_2$ up to a factor of 2 higher than for CO$_2$. Although the RET coefficients show a global tendency to decrease with increasing energy difference between initial and final state, the qualitative RET behaviour, particularly in terms of the efficiency

---

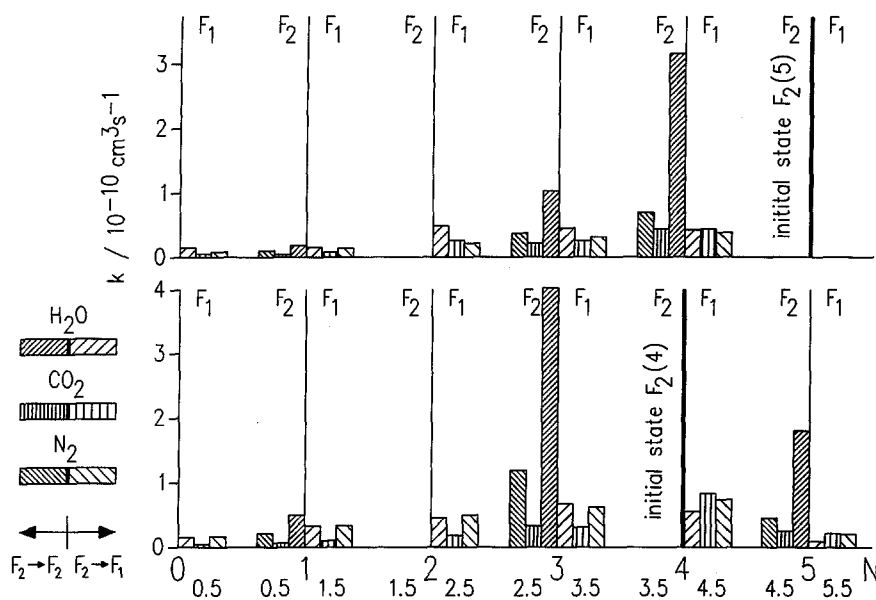[3] In this context, we refer to e/f symmetry according to Alexander et al. [37]

Fig. 1. Rate coefficients at 300 K for rotational energy transfer in thermal collisions of OH ($A^2\Sigma^+$, $v' = 0$) with N_2, CO_2, and H_2O vs rotational quantum number N of the final state. Rate coefficients for symmetry-conserving $F_2 \leftrightarrow F_2$ transitions are grouped to the left side, those for $F_2 \leftrightarrow F_1$ transitions to the right side of each N. The sizes of the bars correspond to the magnitudes of the RET coefficients. top: initial state $F_2(5)$, bottom: initial state $F_2(4)$

Table 1. RET coefficients [$k/10^{-12}$ cm^3 s^{-1}] for thermal collisions of OH ($A^2\Sigma^+$, $v' = 0$) with N_2 at 300 K

Final state	Initial state	
	$F_2(4)$	$F_2(5)$
$F_1(0)$	16.8 ± 1.8	8.48 ± 0.64
$F_2(1)$	21.2 ± 1.4	10.1 ± 1.0
$F_1(1)$	33.5 ± 5.3	14.2 ± 2.0
$F_2(2)$		
$F_1(2)$	50.0 ± 10.7	31.1 ± 2.2
$F_2(3)$	119 ± 21	37.3 ± 2.5
$F_1(3)$	62.4 ± 7.9	31.3 ± 3.1
$F_2(4)$		69.5 ± 4.3
$F_1(4)$	74.5 ± 9.7	38.6 ± 1.2
$F_2(5)$	45.2 ± 2.6	
$F_1(5)$	20.7 ± 1.0	

Table 2. RET coefficients [$k/10^{-12}$ cm^3 s^{-1}] for thermal collisions of OH ($A^2\Sigma^+$, $v' = 0$) with CO_2 at 300 K

Final state	Initial state	
	$F_2(4)$	$F_2(5)$
$F_1(0)$	4.64 ± 0.82	5.40 ± 1.45
$F_2(1)$	6.70 ± 0.89	4.74 ± 0.78
$F_1(1)$	10.4 ± 1.1	8.15 ± 0.92
$F_2(2)$		
$F_1(2)$	18.1 ± 2.7	26.4 ± 3.9
$F_2(3)$	32.7 ± 5.7	21.6 ± 2.5
$F_1(3)$	31.4 ± 3.5	26.0 ± 3.0
$F_2(4)$		43.6 ± 3.5
$F_1(4)$	84.3 ± 5.0	40.6 ± 2.4
$F_2(5)$	25.0 ± 1.5	
$F_1(5)$	21.7 ± 2.2	

of symmetry-changing collisions, is quite different for the three colliders.

The RET coefficients for thermal collisions of OH ($A^2\Sigma^+$, $v' = 0$) with N_2 are given in Table 1. N_2 is the only one of the three collision partners for which a comparison with literature data [31] is possible. Figure 2 shows the RET coefficients of this work (open symbols) together with the data of Lengel and Crosley [31]. For both initial states and for symmetry-changing (circles) as well as symmetry-conserving (squares) collisions, the agreement is in general very good. Although significant discrepancies are observed for the transitions from $F_2(4)$ to $F_2(3)$, $F_1(4)$, and $F_1(5)$, the results from both studies exhibit the same trends: N_2 shows a mild preference for symmetry conservation. The largest RET coefficients are found for transitions with $\triangle J = \triangle N = -1$.

Table 2 reports the RET coefficients for collisions of OH ($A^2\Sigma^+$, $v' = 0$) with CO_2. As also shown in Fig. 1, the coefficients for $F_2 \leftrightarrow F_2$ transitions are in most cases not very different from those for $F_2 \leftrightarrow F_1$ transitions. The most efficient RET process is the almost isoenergetic transfer from $F_2(4)$ to $F_1(4)$ with $\triangle N = 0$, $\triangle J = 1$. Most interestingly,
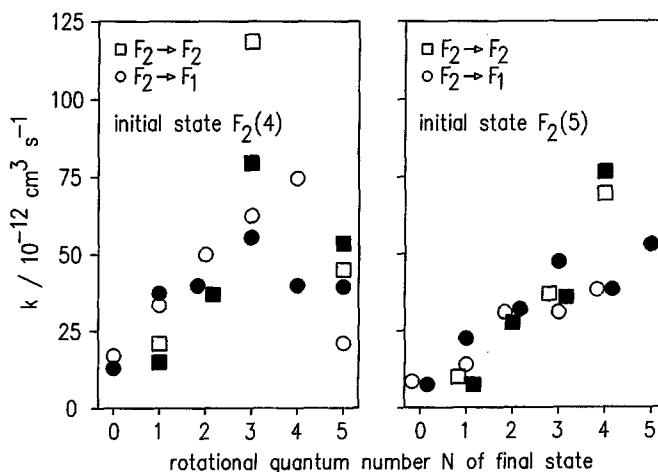

Fig. 2. Rate coefficients at 300 K for rotational energy transfer in thermal collisions of OH ($A^2\Sigma^+$, $v' = 0$) with N_2 vs rotational quantum number N of the final state in comparison with literature. (*open symbols:* this work; *filled symbols:* [31]; *squares:* $F_2 \leftrightarrow F_2$ transitions; *circles:* $F_2 \leftrightarrow F_1$ transitions)

the qualitative and even the quantitative RET behaviour for CO_2 strongly resembles that observed for Ar [29, 30]. Especially for $F_2(4)$ excitation, the individual k_{if} for CO_2 and Ar differ on average by only 15%. The RET in thermal collisions of OH $(A^2\Sigma^+, v' = 0)$ with Ar has been interpreted with respect to ab initio calculations of the interaction potential and the resulting RET coefficients [34, 38]. It seems that the deep wells in the Ar–OH(A) potential can strongly scramble the rotational motion so that the conservation of the F_2 symmetry is unlikely [38]. In contrast, quantum scattering calculations for He–OH(A), where the interaction potential has rather shallow minima and where the long-range part of the potential resembles that of a homonuclear molecule [33, 38], show – in excellent agreement with our experiments [29, 30] – a very strong tendency for symmetry conservation. One might speculate that the CO_2–OH(A) and the Ar–OH(A) potential may possibly exhibit similar features which might account for the extreme similarity in the RET behaviour of these two collision partners.

The RET coefficients for OH $(A^2\Sigma^+, v' = 0)$ with H_2O as collision partner are given in Table 3. A strong propensity for symmetry conservation is observed. This is in accord with results of Smith and Crosley [39] who were among the first to report similar tendencies in flame environments where H_2O was one of the dominant collision partners. Furthermore, transitions with $|\triangle J| = |\triangle N| = 1$ are by far the most efficient ones. For $F_2(4)$ excitation, the two transitions to the adjacent F_2 levels, $F_2(3)$ and $F_2(5)$, account for almost 70% of the total transfer. In comparison, these two coefficients contribute with less than 25% to the total RET out of $F_2(4)$ for CO_2 and about 30% to that for N_2, whereas the almost isoenergetic transition $F_2(4) \leftrightarrow F_1(4)$ accounts for about 35% of the total RET by CO_2, about 15% of that by N_2 and less than 6% of the total RET out of $F_2(4)$ by H_2O.

With the relative efficiency of the total transfer for N_2, CO_2 and H_2O and with typical mole fractions of these three main collision partners in the burnt gases of hydrocarbon/air flames, it can be estimated that RET by N_2 will be at least factors of 2 and 10 more efficient than that by H_2O and CO_2, respectively, provided that the relations between the RET rates are not distorted by different temperature depen-

dencies for these colliders. Lucht et al. [27] report a cross section of $(190 \pm 60) \times 10^{-16}\,\mathrm{cm}^{-2}$, corresponding to a rate coefficient of $(3.5 \pm 1.1) \times 10^{-9}\,\mathrm{cm}^3\mathrm{s}^{-1}$, for the total RET out of the OH $(A^2\Sigma^+, v' = 0, F_2(5)$ level with H_2O as collision partner which they determined in the burnt gases of a 40 mbar $H_2/O_2/N_2$ flame at 1400 K. Although our data set for transfer from $F_2(5)$ is not complete, a crude estimate of the total RET out of this level at 300 K is possible if one assumes a similar RET behaviour as for $F_2(4)$ excitation. It can be concluded from this comparison that the rate coefficient for total RET by H_2O increases with temperature, most probably by about a factor of 3–4 between 300 and 1400 K, which is mainly due to the increase in velocity with temperature.

3 Conclusions and Perspectives

Rate coefficients for state-to-state rotational energy transfer at 300 K for thermal collisions of OH $(A^2\Sigma^+, v' = 0)$ with N_2, CO_2 and H_2O – some of the most important species in hydrocarbon combustion products – have been measured in time-resolved laser-induced fluorescence experiments. As observed in previous investigations [29, 30] for OH $(A^2\Sigma^+, v' = 0)$ with He and Ar as collision partners, the RET does not follow the same pattern for each radical-collider pair. Whereas Ar and CO_2 show almost equally efficient transfer for $F_2 \leftrightarrow F_2$ and $F_2 \leftrightarrow F_1$ transitions, He and H_2O exhibit a distinct and N_2 a slight tendency for symmetry conservation. Upon closer inspection, the detailed features of the RET behaviour exhibit further differences. It seems thus on first glance unlikely that a single physical relationship – as commonly used scaling or fitting laws – would be able to represent all relevant details of the RET of OH$(A^2\Sigma^+, v' = 0)$ by these collision partners. We are currently examining several scaling and fitting laws in connection with the experimental data with the purpose of applying such relations in a global model of the OH collision dynamics [40]. As a realistic model which might be used for the simulation of typical conditions for LIF temperature and concentration measurements also requires information on different vibrational states in OH $(A^2\Sigma^+)$, we have measured state-to-state RET coefficients for $F_2(5)$ excitation in $v' = 1$ [35]. Taking also the investigation on RET in the ground electronic state [32] into account, the previously almost non-existing data base on rotational energy transfer for the OH radical has recently experienced a remarkable improvement. State-specific measurements for various colliders at elevated temperatures would, however, be needed for a more complete picture of the OH RET in combustion system.

Table 3. RET coefficients $[k/10^{-12}\,\mathrm{cm}^3\,\mathrm{s}^{-1}]$ for thermal collisions of OH $(A^2\Sigma^+, v' = 0)$ with H_2O at 300 K

Final state	Initial state	
	$F_2(4)$	$F_2(5)$
$F_1(0)$	15.7 $\pm$ 2.6	14.5 $\pm$ 2.2
$F_2(1)$	49.8 $\pm$ 12.4	18.8 $\pm$ 3.5
$F_1(1)$	32.6 $\pm$ 6.7	15.4 $\pm$ 3.2
$F_2(2)$		
$F_1(2)$	45.3 $\pm$ 12.8	48.9 $\pm$ 5.7
$F_2(3)$	403 $\pm$ 44	103 $\pm$ 20
$F_1(3)$	67.7 $\pm$ 4.9	45.6 $\pm$ 11.0
$F_2(4)$		317 $\pm$ 63
$F_1(4)$	55.4 $\pm$ 5.1	42.3 $\pm$ 5.1
$F_2(5)$	181 $\pm$ 13	
$F_1(5)$	9.64 $\pm$ 1.61	

References

1. A.C. Eckbreth: *Laser Diagnostics for Combustion Temperature and Species,* ed. by A.K. Gupta, D.G. Lilley (Abacus, Tunbridge Wells, UK 1988)

2. R.K. Hanson, J.M. Seitzman, P.H. Paul: Appl. Phys B **50**, 441 (1990)
3. H. Becker, A. Arnold, R. Suntz, P. Monkhouse, J. Wolfrum, R. Maly, W. Pfister: Appl. Phys. B **50**, 473 (1990)
4. P. Andresen, G. Meijer, H. Schlüter, H. Voges, A. Koch, W. Hentschel, W. Oppermann, E. Rothe: Appl. Opt. **29**, 2392 (1990)
5. P.G. Felton, J. Matzaras, D.S. Bomse, R.L. Woodin: SAE Techn. Paper Ser. No. 881631 (1988)
6. N.S. Bergano, P.A. Jaanimagi, M.M. Salour, J.H. Bechtel: Opt. Lett. **8**, 443 (1983)
7. R. Schwarzwald, P. Monkhouse, J. Wolfrum: Chem. Phys. Lett **142**, 15 (1987)
8. M. Schäfer, W. Ketterle, J. Wolfrum: Appl. Phys B **52**, 341 (1991)
9. T. Ni, L.A. Melton: Appl. Spectrosc. **45**, 938 (1991)
10. R.S. Barlow, A. Collignon: 29th Aerospace Sciences Meeting, Reno, AIAA paper 91-0179 (1991)
11. M.P. Lee, P.H. Paul, R.K. Hanson: Opt. Lett. **12**, 75 (1987)
12. P. Andresen, A. Bath, W. Gröger, H.W. Lülf, G. Meijer, J.J. ter Meulen: Appl. Opt. **27**, 365 (1988)
13. R.P. Lucht, D.W. Sweeney, N.M. Laurendeau: Combust. Flame **50**, 189 (1983)
14. K. Kohse-Höinghaus, P. Koczar, Th. Just: 20th Int'l Symp. on Combustion (The Combustion Institute, Pittsburgh, USA 1984) p. 1719
15. J.A. Gray, R.L. Farrow: J. Chem. Phys. **95**, 7054 (1991)
16. C.D. Carter, G.B. King, N.M. Laurendeau: Appl. Opt. Accepted
17. R.P. Lucht, D.W. Sweeney, N.M. Laurendeau: Appl. Opt. **19**, 3295 (1980)
18. D.R. Crosley, G.P. Smith: Combust. Flame **44**, 27 (1982)
19. C. Chan, J.W. Daily: Appl. Opt. **19**, 1357 (1980)
20. J.M. Seitzman: Ph. D. Thesis, HTGL, Stanford University (1991)
21. D.H. Campbell: Appl. Opt. **23**, 689 (1984)
22. D.R. Crosley: J. Phys. Chem. **93**, 6273 (1989)
23. N.L. Garland, D.R. Crosley: 21st Int'l Symp. on Combustion (The Combustion Institute, Pittsburgh, USA 1986) p. 1693
24. R.D. Kenner, S. Pfannenberg, P. Heinrich, F. Stuhl: J. Phys. Chem. **95**, 6585 (1991)
25. M.C. Drake, J.W. Ratcliffe: General Motors Res. Publ. GMR-7426 (1991)
26. D. Stepowski, M.J. Cottereau: J. Chem. Phys. **74**, 6674 (1981)
27. R.P. Lucht, D.W. Sweeney, N.M. Laurendeau: Appl. Opt. **25**, 4086 (1986)
28. J. Burris, J. Butler, T. McGee, W. Heaps: Chem. Phys. **151** (1991)
29. A. Jörg, U. Meier, K. Kohse-Höinghaus: J. Chem. Phys. **93**, 6453 (1990)
30. A. Jörg: Ph. D. Thesis, DLR Stuttgart/Universität Bielefeld (1991)
31. R.K. Lengel, D.R. Crosley: J. Chem. Phys. **67**, 2085 (1977)
32. I.J. Wysong, J.B. Jeffries, D.R. Crosley: J. Chem. Phys. **94**, 7547 (1991)
33. A. Jörg, A. Degli Esposti, H.-J. Werner: J. Chem. Phys. **93**, 8757 (1990)
34. A. Degli Esposti, H.-J. Werner: J. Chem. Phys. **93**, 3351 (1990)
35. R. Kienle, A. Jörg, K. Kohse-Höinghaus: State-to-state RET in OH $(A^2\Sigma^+, v' = 1)$, to be published
36. G.H. Dieke, H.M. Crosswhite: J. Quant. Spectrosc. Radiat. Transfer **2**, 97 (1962)
37. M.H. Alexander, J.E. Smedley, G.C. Corey: J. Chem. Phys. **84**, 3049 (1986)
38. M.H. Alexander, A. Berning, A. Degli Esposti, A. Jörg, A. Kliesch, H.-J. Werner: Ber. Bunsenges. **94**, 1253 (1990)
39. G.P. Smith, D.R. Crosley: 18th Int'l Symp. on Combustion (The Combustion Institute, Pittsburgh, USA 1981) p. 1511
40. R. Kienle, T. Griffin, A. Jörg, K. Kohse-Höinghaus: unpublished results